

# Alpha-particle formation and decay rates from Skyrme-HFB wave functions

D. E. Ward\*, B. G. Carlsson, and S. Åberg

*Mathematical Physics, LTH, Lund University, PO Box 118, S-22100 Lund, Sweden*

PACS REF: 23.60.+e, 21.60.Jz, 21.10.Tg, 27.80.+w

February 11, 2014

## Abstract

$\alpha$  decay is treated microscopically, where the unstable mother nucleus and residual daughter nucleus are described using HFB wave functions, obtained with the Skyrme effective interaction. From these wave functions the amplitude for forming  $\alpha$  particles in the mother nucleus is computed. Two different Skyrme parametrizations with different pairing properties are compared, and we find good agreement with experiment for relative decay rates in both cases. The absolute values of the decay rates are under-estimated.

## 1. Introduction

Nuclear  $\alpha$  decay is the process where an unstable nucleus splits into  ${}^4\text{He}$  ( $\alpha$  particle) and a daughter nucleus with two less protons and two less neutrons. This process is much closer related to spontaneous fission, i.e., a disintegration of the nucleus into two nuclei with mass numbers  $A \gtrsim 60$ , than  $\beta$  and  $\gamma$  decay, which involve the creation of particles due to the interaction of the nucleus with weak and electromagnetic fields, respectively.

For superheavy elements (SHE) fission and  $\alpha$  decay are the dominant decay modes. The detection of emitted  $\alpha$  particles has been the principal method of identifying SHEs, created in heavy ion fusion reactions [1]. By detecting  $\alpha$  particles from decays leaving the daughter nucleus in an excited state in coincidence with the subsequent electromagnetic decay, a first exploration of nuclear level structure as well as possible identification by X-ray emission in the  $Z = 115$  region was recently made in the experiment of Ref. [2]. Such  $\alpha$  decays populating excited daughter states occur due to different structure of mother and daughter nuclei, that hinders the decay to the ground state [3].

Both fission and  $\alpha$ -decay modes proceed through classically forbidden regions of configuration space, i.e., if the motion of the nucleons is described by some collective coordinates, the nuclear wave function must tunnel through a potential barrier parametrized by these coordinates. For fission the collective coordinates usually characterize the evolution of the overall nuclear shape, while for  $\alpha$  decay one can choose the distance between the center of mass of

the daughter nucleus and the  $\alpha$  particle.

The tunneling leads to the huge variation in  $\alpha$ -decay lifetimes across the nuclear chart, as the half-life depends roughly exponentially on the difference between the height of the barrier and the  $Q_\alpha$  value. Due to the barrier penetration being the dominant factor determining the decay probability, this dependence on  $Q_\alpha$  can be described using phenomenological  $\alpha$ -daughter potentials or semi-empirical formulas. Within such approaches one has been able to reproduce the overall trends in  $\alpha$ -decay half-lives using a small number of free parameters [4, 5].

To connect  $\alpha$  decay with other nuclear observables, and describe the hindrance of certain  $\alpha$ -decay channels, a microscopic model is needed. In a microscopic description one considers interacting nucleons, and the formation of an  $\alpha$ -daughter configuration from the initial state of the mother nucleus. A predictive description of both nuclear ground state and  $\alpha$ -decay properties based on the same effective interaction is a challenging task for theory. Most microscopic calculations have been based on either a phenomenological Woods-Saxon or Nilsson mean field combined with BCS pairing [3, 6, 7], or a shell-model type description where four nucleons interact with the daughter nucleus and each other through effective model space interactions [8, 9, 10].

In this work we use well-tested effective Skyrme interactions to describe the nuclear structure. The wave functions of the mother and daughter nuclei are obtained self consistently using the Hartree-Fock-Bogoliubov (HFB) method. The Skyrme-HFB approach provides a reasonable description of ground state observables such as binding energies and densities throughout the nuclear chart [11].

In [12] we performed extensive calculations for even even near-spherical nuclei using the SLy4 effective Skyrme interaction. In this work we explore if comparable results are obtained using a different modern Skyrme parametrization, UNEDF1 [13]. The connection between the two-particle transfer density, the pairing density and the probability of forming  $\alpha$  particles is discussed. Also new for this work is the investigation of the accuracy of the  $\delta$ -function approximation [14], which drastically reduces the time to compute the  $\alpha$ -particle formation amplitude, by comparing with the full calculation in the small  $\alpha$ -particle

\*e-mail: [daniel.ward@matfys.lth.se](mailto:daniel.ward@matfys.lth.se)

limit.

The contribution is organized as follows. In Sec. 2 the  $\alpha$ -decay formalism and the nuclear structure model are briefly introduced. In Sec. 3 the convergence of the numerical results, and the  $\delta$ -function approximation are investigated. We discuss the role of pairing correlations in section 4. Results for Po, Ra, and Rn isotopes are compared with experiment in Sec. 5. Finally, in Sec. 6 we present our conclusions.

## 2. Theory

We use the same decay formalism and Skyrme-HFB nuclear structure model as in the previous work [12], where several aspects of the approach and the introduced approximations are discussed in detail. Here we recapitulate only the ingredients necessary for the discussion of the current results.

### 2.1. Decay formalism

$\alpha$ -decay is described in the microscopic  $R$ -matrix approach [15, 16, 17]. The amplitude of the decay process depends on the overlap of the mother ( $M$ ) nucleus with a daughter ( $D$ ) and  $\alpha$  cluster, called the *formation amplitude* [15],

$$g_L(r_{\alpha D}) = \int \mathcal{A} \left[ \Phi_J^{(D)}(\xi_D), \Phi_0^{(\alpha)}(\xi_\alpha) Y_L(\hat{r}_{\alpha D}) \right]_{IM}^* \quad (1)$$

$$\times \Psi_{IM}^{(M)}(\xi_M) d\xi_D d\xi_\alpha d\hat{r}_{\alpha D},$$

where  $L$  is the angular momentum,  $\Psi_{IM}^{(M)}(\xi_M), \Phi_J^{(D)}(\xi_D)$ , and  $\Phi_0^{(\alpha)}(\xi_\alpha)$  are the mother, daughter and  $\alpha$  particle wave functions, respectively,  $\xi_i$  are intrinsic coordinates for nucleus  $i$ , and  $\mathbf{r}_{\alpha D}$  is the distance between the centers of mass of the daughter nucleus and  $\alpha$  particle. In this work we consider the g.s. to g.s.  $\alpha$  decay in even-even nuclei implying  $L = J = I = 0$ .

The decay width is given by [15],

$$\Gamma(r_c) = 2\gamma_0^2(r_c) P_0(Q_\alpha, r_c), \quad (2)$$

where  $P_0$  is the Coulomb penetrability, and  $\gamma_0$  is the reduced width,

$$\gamma_0^2(r_c) = \frac{\hbar^2}{2\mu r_c} r_c^2 g_0^2(r_c), \quad (3)$$

with the reduced mass  $\mu$ . The penetrability depends strongly on  $Q_\alpha$ . A variation of  $\pm 1$  MeV can produce a variation of several orders of magnitude in the penetrability. To avoid this we use the experimental value,  $Q_\alpha^{\text{exp}}$ .

The reduced width and the penetrability entering Eq. (2) both depend on the matching radius  $r_c$ , that should be chosen beyond the range of inter-cluster nuclear forces. If the formation amplitude has a tail proportional to an outgoing Coulomb wave function corresponding to the correct energy  $Q_\alpha^{\text{exp}}$ , the decay width  $\Gamma$  becomes constant for large  $r_c$ . For an approximate nuclear structure model there might thus be some  $r_c$  dependence of  $\Gamma$ .

### 2.2. Nuclear structure model

The g.s. wave functions of mother and daughter nuclei are obtained from spherically symmetric solutions to the HFB equations, solved in a large spherical oscillator basis using an extended version of the program HOSPHE(v1.02) [18]. In the particle-hole (p-h) channel the effective Skyrme forces SLy4 and UNEDF1 are used.

In the particle-particle (p-p) channel an effective density-dependent contact interaction [19] is used,

$$V_{\text{pair}}^q(\mathbf{r}, \mathbf{r}') = V_q \left[ 1 - \beta \frac{\rho(\mathbf{r})}{\rho_c} \right] \delta(\mathbf{r} - \mathbf{r}'), \quad q = p, n, \quad (4)$$

where the parameters  $V_q$  and  $\beta$  determine the strength and density dependence of the interaction, and  $\rho_c$  is the saturation density of nuclear matter, taken as  $\rho_c = 0.16 \text{ fm}^{-3}$ . The interaction is regularized by a truncation in the equivalent spectra [20] at 60 MeV. To avoid a collapse of the pairing in nuclei close to closed shells an approximate version of the Lipkin-Nogami method [20] is used. The Skyrme force SLy4 is used in combination with volume-type ( $\beta = 0$ ), and surface-type pairing ( $\beta = 1$ ), with the pairing strengths used in [12]. For UNEDF1 we use the mixed pairing ( $\beta = \frac{1}{2}$ ) obtained in the simultaneous fit of the p-h and p-p effective interactions performed in [13].

We use the standard approximation for the  $\alpha$  particle wave function [15, 21],

$$\Phi_{00}^{(\alpha)}(\mathbf{r}_\pi, \mathbf{r}_\nu, \mathbf{r}_\alpha, s_1, s_2, s_3, s_4) = \left( \frac{4}{b_\alpha^3 \sqrt{\pi}} \right)^{3/2} e^{-\frac{r_\pi^2 + r_\nu^2 + r_\alpha^2}{2b_\alpha^2}} \times \left( \frac{1}{\sqrt{4\pi}} \right)^3 \quad (5)$$

$$\times [\chi_{\frac{1}{2}}(s_1), \chi_{\frac{1}{2}}(s_2)]_{00} [\chi_{\frac{1}{2}}(s_3), \chi_{\frac{1}{2}}(s_4)]_{00},$$

where  $b_\alpha$  is a size parameter, chosen as  $b_\alpha = 1.41 \text{ fm}$ ,  $s_1, s_2$  are spin coordinates for the two protons, and  $s_3, s_4$  for the two neutrons. The coordinates  $\mathbf{r}_\pi, \mathbf{r}_\nu, \mathbf{r}_\alpha$  are related to the coordinates of the two protons  $\mathbf{r}_1, \mathbf{r}_2$  and of the two neutrons  $\mathbf{r}_3, \mathbf{r}_4$  through,  $\mathbf{r}_\pi = (\mathbf{r}_1 - \mathbf{r}_2)/\sqrt{2}$ ,  $\mathbf{r}_\nu = (\mathbf{r}_3 - \mathbf{r}_4)/\sqrt{2}$ ,  $\mathbf{r}_\alpha = \frac{1}{2}(\mathbf{r}_1 + \mathbf{r}_2 - \mathbf{r}_3 - \mathbf{r}_4)$ . The center of mass coordinate for the four nucleons is,  $\mathbf{R} = \frac{1}{4}(\mathbf{r}_1 + \mathbf{r}_2 + \mathbf{r}_3 + \mathbf{r}_4)$ .

### 2.3. Calculation of the formation amplitude

The formation amplitude (1) is obtained by expanding the mother nucleus in terms of the daughter and valence nucleons [15], and integrating over daughter coordinates,

$$g_0(R) = \frac{1}{\sqrt{4\pi}} \int \Phi_{00}^{(\alpha)*}(r_\pi, r_\nu, r_\alpha) \Phi^{(v)}(\mathbf{r}_1, \mathbf{r}_2, \mathbf{r}_3, \mathbf{r}_4) d\xi_\alpha d\hat{R}, \quad (6)$$

where  $\mathbf{R}$  is the center of mass coordinate for the nucleons of the  $\alpha$  particle, and  $\Phi^{(v)} = \sqrt{8} \Phi^{(v_p)}(\mathbf{r}_1, \mathbf{r}_2) \Phi^{(v_n)}(\mathbf{r}_3, \mathbf{r}_4)$  is the valence nucleon wave function. The factor of  $\sqrt{8}$  is the renormalization of a wave function obtained for the

coordinates  $\mathbf{r}_1, \mathbf{r}_2, \mathbf{r}_3, \mathbf{r}_4$ , when used as a wave function in the coordinates  $\mathbf{r}_\pi, \mathbf{r}_\nu, \mathbf{r}_\alpha, \mathbf{R}$  [22]. A few approximations are made to get this simpler expression, discussed in [12]. If the daughter nucleus is heavy compared to the  $\alpha$  particle, and their relative distance,  $R$ , is large so that they have little spatial overlap, the errors introduced by these approximations are estimated to be small.

The two-proton,  $q = \pi$ , and two-neutron parts,  $q = \nu$ , of the valence nucleon wave function are given by,

$$\Phi^{(v_q)}(\mathbf{r}_a, \mathbf{r}_b) = \frac{1}{2} \sum_{lj} \sum_{nn'} \hat{j} B_{lj;nn'}^q \times \mathcal{A}\{\phi_{nlj}(\mathbf{r}_a), \phi_{n'lj}(\mathbf{r}_b)\}_{00}, \quad (7)$$

where  $\phi_{nlj}$  are harmonic oscillator eigenfunctions with  $n$  nodes, orbital and total angular momentum  $l$  and  $j$ , respectively. Since proton-neutron pairing is not considered the HFB wave functions splits into proton and neutron parts. The expansion coefficients  $B^q$  are given by the overlap of the corresponding proton or neutron parts of the daughter HFB vacuum with two particle-annihilation operators acting on the mother HFB vacuum,

$$B_{k,k'}^q = \langle D^q | a_{k'} a_k | M^q \rangle. \quad (8)$$

The formation amplitude (6) is subsequently evaluated by transforming the valence wave function to relative and center of mass coordinates using Talmi-Moshinsky oscillator brackets [23].

### 3. Numerical application

#### 3.1. Convergence

The matching radius,  $r_c$ , in the  $R$ -matrix decay width expression (2) must be chosen in the region where nuclear forces between the alpha particle and the daughter nucleus are negligible. In the case of  $^{212}\text{Po}$  this means [12] that the formation amplitude should be converged for separations  $R \leq 10$  fm. As seen in Fig. 1 this is fulfilled when  $N_{max} \geq 20$ , where the oscillator basis consists of all major shells up to and including  $N_{max}$ . In this work we use, unless otherwise noted,  $N_{max} = 30$  throughout.

#### 3.2. $\alpha$ particle wave function - small size limit

The evaluation of the formation amplitude (6), involves the computationally expensive evaluation of overlap integrals in relative coordinates. Within the  $\delta$ -function approximation [14], these computations are avoided, reducing the computational time by at least two orders of magnitude. The error introduced vary from nuclei to nuclei, partly due to that the contribution from high- $j$  orbitals is exaggerated [14], and the approximation has generally not been used in recent works. To better understand how the errors are introduced, we investigate the formation amplitude in the small  $\alpha$ -particle limit.

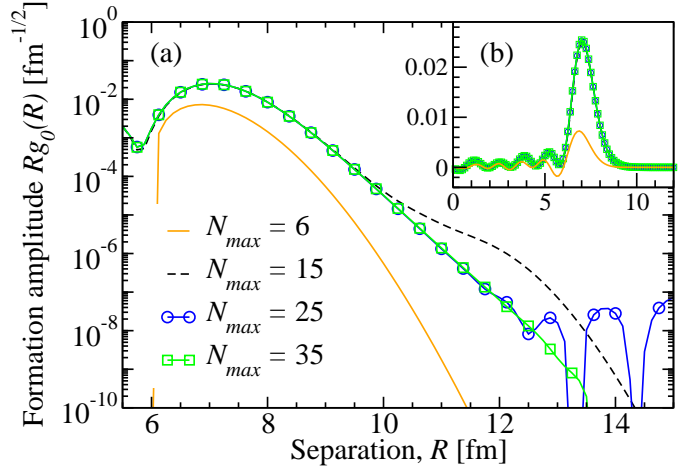


Figure 1: Convergence of the formation amplitude. (a) shows the tail of the formation amplitude in logarithmic scale. (b) shows the formation amplitude in linear scale, only the  $N_{max} = 6$  results differ from the rest in this scale.

The  $\delta$ -approximation consists in assuming the valence wave function in the coordinates  $r_\pi, r_\nu, r_\alpha$  be constant over the size of the  $\alpha$  particle,

$$\Phi^{(v)}(\mathbf{r}_\pi, \mathbf{r}_\nu, \mathbf{r}_\alpha, \mathbf{R}) \approx \Phi^{(v)}(0, 0, 0, \mathbf{R}) = \sqrt{8} \Phi^{(v_\pi)}(\mathbf{R}, \mathbf{R}) \Phi^{(v_\nu)}(\mathbf{R}, \mathbf{R}). \quad (9)$$

Inserting into Eq. (6) gives,

$$g_0(R) \approx \int \Phi_{00}^{(\alpha)*}(\mathbf{r}_\pi, \mathbf{r}_\nu, \mathbf{r}_\alpha) d\xi_\alpha \times \sum_{s_1 \dots s_4} \int \Phi_{00}^{(\alpha)*}(s_1, \dots, s_4) Y_{00}^*(\hat{R}) \times \Phi^{(v)}(0, 0, 0, \mathbf{R}; s_1, \dots, s_4) d\hat{R}, \quad (10)$$

where the  $\alpha$  particle wave function is separated into spin and position coordinates, and the summation over spins is shown explicitly. The first integral gives the prefactor,

$$A(b_\alpha) \equiv \int \Phi_{00}^{(\alpha)*}(\mathbf{r}_\pi, \mathbf{r}_\nu, \mathbf{r}_\alpha) d\xi_\alpha = (2b_\alpha \sqrt{\pi})^{9/2}. \quad (11)$$

This factor differs slightly from the one in [14].

Performing the summation over spins, and the angular integration, the formation amplitude becomes,

$$g_0(R) \approx \sqrt{32\pi} A(b_\alpha) \langle D^\pi | M^\pi \rangle \langle D^\nu | M^\nu \rangle \times \kappa_\pi^{DM}(\mathbf{R}) \kappa_\nu^{DM}(\mathbf{R}), \quad (12)$$

where  $\kappa_q^{DM}(\mathbf{R})$  is the two-particle transfer density, here defined as,

$$\kappa_q^{DM}(\mathbf{R}) \equiv \frac{\langle D^q | a(\mathbf{R}, \downarrow) a(\mathbf{R}, \uparrow) | M^q \rangle}{\langle D^q | M^q \rangle}, \quad q = \pi, \nu. \quad (13)$$

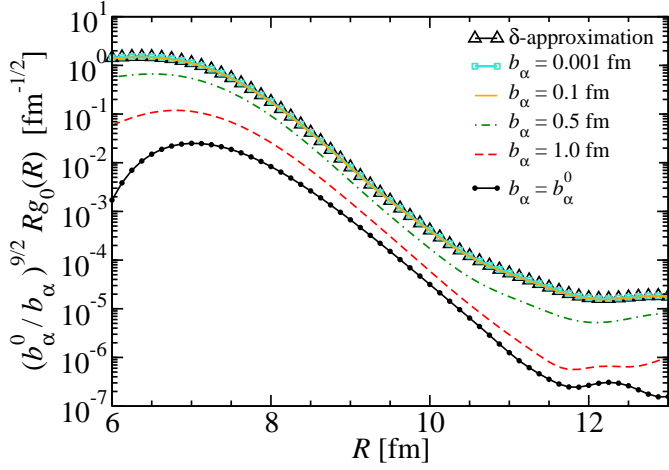


Figure 2: Formation amplitude for  $^{212}\text{Po}$  calculated for  $\alpha$  particle wave functions of different sizes  $b_\alpha$ , and rescaled, compared to the result of the  $\delta$ -function approximation.

The formation amplitude in the  $\delta$ -function approximation, using Eq. (12), is compared to the result of the full calculation, Eq. (6), for the  $\alpha$  decay of  $^{212}\text{Po}$  in Fig. 2. The HFB wave functions are obtained with SLy4 and volume pairing, and oscillator shells up to  $N_{max} = 20$  are included. To investigate for what size of  $\alpha$  particle the assumption of the  $\delta$ -function approximation is valid, the results of full calculations using an  $\alpha$  particle wave function with size parameter  $b_\alpha$ , smaller than the standard value of  $b_\alpha^0 = 1.41$  fm, are also shown. The results are scaled by the factor  $(b_\alpha^0/b_\alpha)^{9/2}$ , so that a constant valence-nucleon wave function will produce the same formation amplitude regardless of  $b_\alpha$ .

The  $\delta$ -function approximation over-estimates the formation amplitude by a factor of 10 or more. From the results of calculations with decreasing  $b_\alpha$  we note that this overestimation is due to the neglect of the decrease of the valence-nucleon wave function with increasing distance between nucleons  $r_\pi, r_\nu, r_\alpha$ . As the volume in which the valence-nucleon wave function is sampled, controlled by the parameter  $b_\alpha$ , is decreased the results tend to the results of the  $\delta$ -function approximation.

We conclude that the  $\delta$ -approximation is not sufficiently accurate. More work is needed to find a suitable approximation to reduce the computational time. For the remaining calculations we shall use the full expression (6) for the formation amplitude.

#### 4. Pairing correlations

The formation amplitude depends strongly on the magnitude of the pairing correlations. For BCS type calculations a strong dependence on the pairing gap was demonstrated in e.g. [6], and a similar dependence was observed in the HFB case [12].

The  $R$ -matrix decay width for  $^{212}\text{Po}$  calculated using different effective Skyrme and pairing interactions is shown

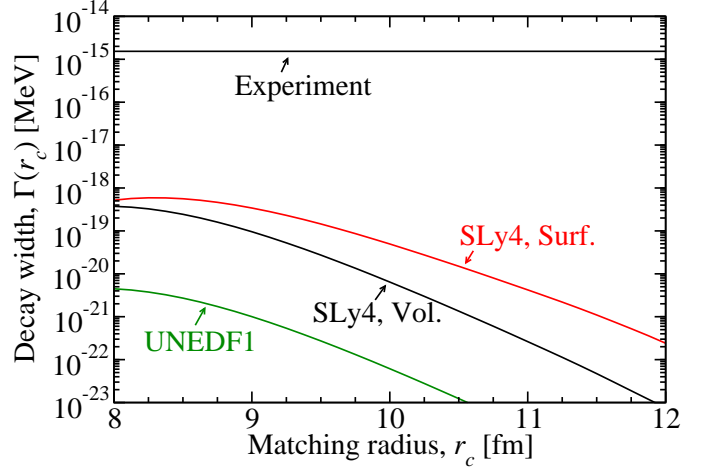


Figure 3:  $R$ -matrix decay width for  $^{212}\text{Po}$ , obtained using different effective interactions.

in Fig. 3. As can be seen in the figure all considered interactions produce too small decay widths to reproduce experimental data. SLy4 with a surface pairing force yields the largest values, whereas the UNEDF1 produces the smallest decay width. The slope of  $\Gamma(r_c)$  as a function of matching radius  $r_c$  indicates that the model predicts an  $\alpha$  particle more bound to the daughter compared to experiment.

While both SLy4 results are obtained using a pairing that gives lowest quasi-particle energies,  $E_q^{\min}$ , close to the three-point mass differences,  $\Delta_p^{\text{exp}}(^{212}\text{Po}) = 0.765$  MeV, and  $\Delta_n^{\text{exp}}(^{212}\text{Po}) = 0.766$  MeV, the UNEDF1 produces smaller pairing,  $E_p^{\min}(^{212}\text{Po}) = 0.144$  MeV,  $E_n^{\min}(^{212}\text{Po}) = 0.111$  MeV. This pairing produces the much smaller decay width in this case.

The connection between the pairing and the formation amplitude can be seen more clearly in the  $\delta$ -function approximation, Eq. (12). In this approximation the formation amplitude is proportional to the product of the pair-transfer densities  $\kappa_p^{DM}(\mathbf{R})\kappa_n^{DM}(\mathbf{R})$ . Fig. 4 compares the pairing density,  $\kappa_q(\mathbf{r}) = \langle M^q | a(\mathbf{r}, \downarrow) a(\mathbf{r}, \uparrow) | M^q \rangle$ , and the two-nucleon transfer density,  $\kappa_q^{DM}(\mathbf{r})$ , Eq. (13), calculated in the three model parametrizations for  $^{212}\text{Po}$ . It is interesting to note that for all three cases the transfer density seem to be well approximated by the pairing density for large radii. The surface pairing has the largest tail of the pair density, while the UNEDF1 pairing density is overall much smaller due to the smaller pairing. This behavior explains qualitatively the  $R$ -matrix decay widths in Fig. 3.

#### 5. Results for $\alpha$ -decay properties of Po, Rn, Ra isotopes

Calculations for  $\alpha$ -decay widths of all even-even near-spherical  $\alpha$  emitters included in the compilation of experimental data of [24] were performed using the SLy4 Skyrme force in [12]. Here we focus on the results for the



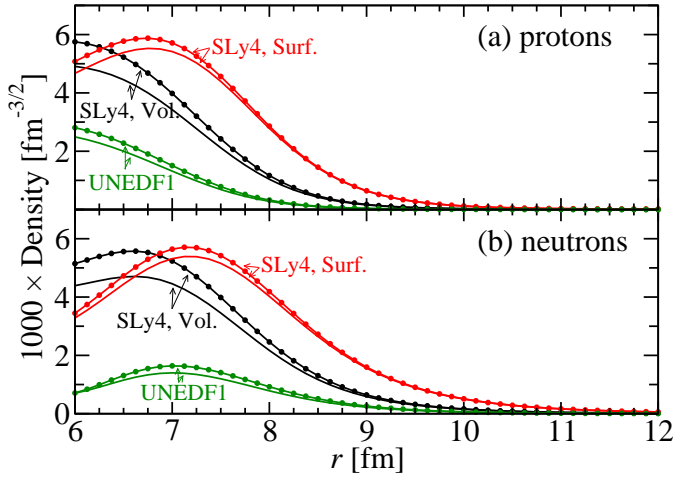


Figure 4: Pairing density (solid lines), and two-nucleon transfer density (dotted lines) for  $^{212}\text{Po}$ .

Table 1: Mean,  $\mathcal{M}$ , and standard deviation,  $\sigma$ , of  $\log_{10}[\gamma^2(r_t)/\gamma_{\text{exp}}^2(r_t)]$  for the 27 studied Po, Rn and Ra isotopes.

Model	$\mathcal{M}$	$\sigma$
SLy4, Volume pairing	-3.7897	0.3162
SLy4, Surface pairing	-3.1409	0.2213
UNEDF1	-5.7080	0.2278
UDL	0.2111	0.3788

27 near-spherical Po, Rn, and Ra isotopes, and compare with results using the UNEDF1 effective interaction.

To compare the microscopic  $\alpha$ -decay properties for several nuclei we investigate the reduced width,  $\gamma^2(r_c)$ , Eq. (3), at  $r_c = r_t$ , with the touching radius  $r_t = r_0 [(A-4)^{1/3} + 4^{1/3}]$ , where  $A$  is the mass number of the mother nucleus and  $r_0 = 1.2$  fm.  $r_t$  gives the approximate separation at the  $\alpha$ -daughter nucleus touching configuration.

For g.s. to g.s.  $\alpha$  decay of even spherical nuclei, the experimental reduced width is defined as,

$$\gamma_{\text{exp}}^2(r_t) = \frac{\Gamma_{\text{exp}}}{2P_0(Q_{\alpha}^{\text{exp}}, r_t)}, \quad (14)$$

where  $\Gamma_{\text{exp}} = \hbar \ln 2 / T_{1/2}^{\text{exp}}$  is the partial decay width for the g.s. to g.s. decay channel and  $P_0$  is the Coulomb penetrability.

Tab. 1 shows the mean  $\mathcal{M}$  and standard deviation  $\sigma$  of the logarithm of theoretical reduced widths divided by the corresponding experimental value for the 27 isotopes,

$$\log_{10} \left[ \frac{\gamma^2(r_t)}{\gamma_{\text{exp}}^2(r_t)} \right] = \log_{10} \left[ \frac{\Gamma(r_t)}{\Gamma_{\text{exp}}} \right]. \quad (15)$$

For comparison results from the semi-empiric formula, Universal Decay Law (UDL), of Ref [4] are included. One notes that the microscopic models produce reduced widths which are on average 3 or more orders of magnitude

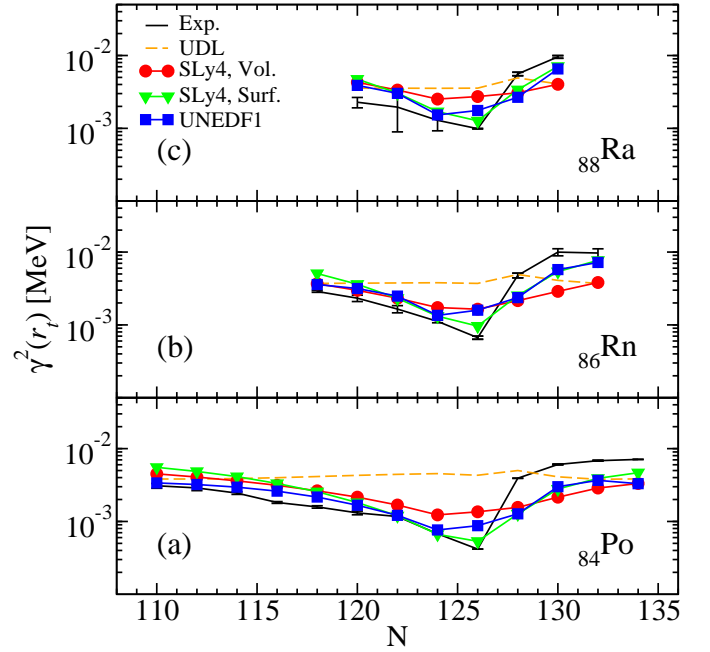


Figure 5: Reduced widths at the touching radius, as a function of the mother nucleus neutron number. The error bars show experimental values, the dashed line results from the UDL formula. The circles, triangles and squares show results from microscopic HFB calculations using different effective interactions. The microscopic results are normalized with the constant factor  $10^{-\mathcal{M}}$ .

smaller than experiment, whereas the UDL produces on the average a good agreement with data. The spread,  $\sigma$ , around this mean is, on the other hand, smaller for the microscopic models, with the smallest deviation for the SLy4 + Surface pairing and the UNEDF1 effective interactions.

The reduced widths are compared with experiment in Fig. 5. For each of the microscopic models the results are normalized with the constant  $10^{-\mathcal{M}}$ . From the figure it is apparent that the normalized microscopic results (circles, triangles, and squares) follow the variation of  $\gamma_{\text{exp}}^2(r_t)$  better than the semi-empiric model (dashed line), that does not take into account the nuclear structure.

Reduced  $\alpha$ -decay widths along the Po, Rn and Ra isotope chains show a similar behavior: As the neutron number is increased, the reduced width decreases rather smoothly until the neutron shell closure at  $N = 126$ , after which the experimental value increases drastically across the shell gap. For  $N \geq 128$  the reduced widths again increase in a smooth way as  $N$  is increased. None of the models fully capture the magnitude of the increase in reduced width when crossing the gap. The best agreement is for SLy4, with surface type pairing. For all microscopic models most of the variation with neutron number is reasonably reproduced.

This shows that although the magnitude of the calculated formation amplitudes are much too small, the missing nuclear structure effects needed to reproduce data is

roughly proportional to the HFB results for all three considered model parametrizations.

The reduced width  $\gamma^2(r_c)$  depends on the matching radius  $r_c$ , and decreases with increasing values of this parameter, as the tail of the formation amplitude decreases inside the Coulomb barrier. As noted in Sec. 4 the decrease of the microscopic reduced width is more rapid than the corresponding experimental values, causing the theoretical decay widths  $\Gamma(r_c)$ , shown in Fig. 3, to decrease with  $r_c$ . This implies that the HFB results presented in Tab. 1 and Fig. 5 depend on the choice of  $r_c$ . To test the sensitivity of the results to  $r_c$  we use a scaled touching radius  $r'_t$  with  $r_0 = 1.5$  fm. While the mean values decrease by about 2 orders of magnitude, the relative values still show a good agreement with data, reflected in small changes in the standard deviations  $\sigma$ .

## 6. Conclusions

The magnitude of the reduced  $\alpha$ -decay widths turned out to be on average 5.7 orders of magnitude too small compared to experiment for the UNEDF1, whereas the SLy4 wave functions produced 3-4 orders too small amplitudes. The much smaller UNEDF1 values are mainly due to the weaker pairing.

The three considered model parametrizations have quite different pairing properties. In spite of this all three provide relative decay rates that are in good agreement with data. The good agreement for the normalized widths indicates that the missing effects needed to reproduce absolute values of experimental decay rates seem to be roughly proportional to the Skyrme-HFB results.

To describe these missing effects it is likely that one has to go beyond the HFB level and introduce other types of correlations. Such a model would require more complicated wave functions, that might make the calculation of the formation amplitudes intractable. A great reduction in computer time can be achieved if the computation of overlap integrals in relative coordinates can be avoided, which is the case in the  $\delta$ -function approximation. From our investigation we note that this approximation is too drastic, as the valence nucleon wave function has appreciable variation across the size of the  $\alpha$  particle.

## References

- [1] Y. Oganessian. *J. Phys G*, 34:R165, 2007.
- [2] D. Rudolph et al. *Phys. Rev. Lett.*, 111:112502, 2013.
- [3] J. K. Poggenburg, H. J. Mang, and J. O. Rasmussen. *Phys. Rev.*, 181:1697, 1969.
- [4] C. Qi et al. *Phys. Rev. C*, 80:044326, 2009.
- [5] A. Zdeb, M. Warda, and K. Pomorski. *Phys. Rev. C*, 87:024308, 2013.
- [6] D. S. Delion, A. Insolia, and R. J. Liotta. *Phys. Rev. C*, 54:292.
- [7] A. Insolia, R. J. Liotta, and E. Maglione. *Europhys. Lett.*, 7:209, 1988.
- [8] I. Tonozuka and A. Arima. *Nucl. Phys.*, A323:45, 1979.
- [9] D. S. Delion and J. Suhonen. *Phys. Rev. C*, 61:024304, 2000.
- [10] R. Id Betan and W. Nazarewicz. *Phys. Rev. C*, 86:034338, 2012.
- [11] M. Bender, P.-H. Heenen, and P.-G. Reinhard. *Rev. Mod. Phys.*, 75:121.
- [12] D. E. Ward, B. G. Carlsson, and S. Åberg. *Phys. Rev. C*, 88:064316, 2013.
- [13] M. Kortelainen et al. *Phys. Rev. C*, 85:024304, 2012.
- [14] J. O. Rasmussen. *Nuclear Physics*, 44:93, 1963.
- [15] R. G. Lovas et al. *Phys. Rep.*, 294:265, 1998.
- [16] H.-D. Zeh. *Z. Phys.*, 175:490, 1963.
- [17] H. J. Mang. *Ann. Rev. Nucl. Sci.*, 14:1, 1964.
- [18] B. G. Carlsson et al. *Comp. Phys. Commun.*, 181:1641, 2010.
- [19] J. Dobaczewski and P. Olbratowski. *Comp. Phys. Commun.*, 158:158, 2004.
- [20] M. V. Stoitsov et al. *Comp. Phys. Commun.*, 167:43, 2005.
- [21] D. S. Delion. Number 819 in Lecture notes in physics. Springer, 2010.
- [22] J. Eichler and H.-J. Mang. *Z. Phys.*, 183:321, 1965.
- [23] G. P. Kamuntavičius et al. *Nucl. Phys.*, A695:191, 2001.
- [24] Y. A. Akovali. *Nuclear Data Sheets*, 84:1, 1998.